eNeuro

Research Article: New Research | Disorders of the Nervous System

Overexpression of Parkinson's Disease-Associated Mutation LRRK2 G2019S in Mouse Forebrain Induces Behavioral Deficits and α-Synuclein Pathology

LRRK2 G2019S behavior and α-synuclein pathology

Yulan Xiong[1,2,8], Stewart Neifert[1,2], Senthilkumar S. Karuppagounder[1,2], Jeannette N. Stankowski[1,2], Byoung Dae Lee[1,2], Jonathan C. Grima[1,2,3], Guanxing Chen[8], Han Seok Ko[1,2], Yunjong Lee[1,2], Debbie Swing[9], Lino Tessarollo[9], Ted M. Dawson[1,2,3,5,6,7] and Valina L. Dawson[1,2,3,4,6,7]

[1]*Neuroregeneration and Stem Cell Programs, Institute for Cell Engineering*

[2]*Department of Neurology*

[3]*Soloman H. Snyder Department of Neuroscience*

[4]*Department of Physiology*

[5]*Department of Pharmacology and Molecular Sciences, Johns Hopkins University School of Medicine, Baltimore, MD 21205, USA*

[6]*Adrienne Helis Malvin Medical Research Foundation*

[7]*Diana Helis Henry Medical Research Foundation, New Orleans, LA 70130, USA 2685*

[8]*Department of Anatomy and Physiology, Kansas State University College of Veterinary Medicine, Manhattan, KS 66506, USA*

[9]*N, Eural Development Section, Mouse Cancer Genetics Program, Center for Cancer Research, National Cancer Institute, Frederick, MD 21702, USA*

DOI: 10.1523/ENEURO.0004-17.2017

Received: 4 January 2017

Revised: 27 February 2017

Accepted: 1 March 2017

Published: 6 March 2017

Author Contributions: X., H.S.K., T.M.D. and V.L.D. Designed Research; Y.X., S.N., S.S.K., J.N.S., B.D.L., J.C.G., G.C., Y.L., D.S., and L.T. Performed research and Analyzed Data; Y.X., S.N., T.M.D. and V.L.D. Wrote the Paper.

Funding: HHS | NIH | National Institute on Aging (NIA), Funder Id: 100000049; Grant Id: AG046366

Funding: HHS | NIH | National Institute of Neurological Disorders and Stroke (NINDS): Funder Id: 100000065; Grant Ids: NS082205 and NS38377.

Conflict of Interest: Authors report no conflict of interest.

Correspondence should be addressed to either Valina L. Dawson (Lead Contact), Neuroregeneration and Stem Cell Programs, Institute for Cell Engineering, Department of Neurology, Johns Hopkins University School of Medicine, 733 N. Broadway, MRB 731, Baltimore, MD 21205, USA, E-mail: vdawson@jhmi.edu or Yulan Xiong, Department of Anatomy and Physiology, Kansas State University College of Veterinary Medicine, 212 Coles Hall, Manhattan, KS 66506, USA, E-mail: yulanxiong@ksu.edu

Cite as: eNeuro 2017; 10.1523/ENEURO.0004-17.2017

1. Manuscript Title:
Overexpression of Parkinson's disease-associated mutation LRRK2 G2019S in mouse forebrain induces behavioral deficits and α-synuclein pathology

2. Abbreviated Title:
LRRK2 G2019S behavior and α-synuclein pathology

3. List all Author Names and Affiliations in order as they would appear in the published article:

Yulan Xiong[1,2,8*], Stewart Neifert[1,2], Senthilkumar S. Karuppagounder[1,2], Jeannette N. Stankowski[1,2,$], Byoung Dae Lee[1,2,#], Jonathan C. Grima[1,2,3], Guanxing Chen[8], Han Seok Ko[1,2], Yunjong Lee[1,2,&], Debbie Swing[9], Lino Tessarollo[9], Ted M. Dawson[1,2,3,5,6,7] and Valina L. Dawson[1,2,3,4,6,7*]

[1]Neuroregeneration and Stem Cell Programs, Institute for Cell Engineering,
[2]Department of Neurology,
[3]Soloman H. Snyder Department of Neuroscience,
[4]Department of Physiology
[5]Department of Pharmacology and Molecular Sciences, Johns Hopkins University School of Medicine, Baltimore, MD 21205, USA
[6]Adrienne Helis Malvin Medical Research Foundation,
[7]Diana Helis Henry Medical Research Foundation, New Orleans, LA 70130-2685, USA
[8]Department of Anatomy and Physiology, Kansas State University College of Veterinary Medicine, Manhattan, KS 66506, USA
[9]Neural Development Section, Mouse Cancer Genetics Program, Center for Cancer Research, National Cancer Institute, Frederick, MD 21702, USA

[#]Current address: Age-Related and Brain Disease Research Center, Department of Neuroscience, Kyung Hee University, Seoul 130-701, South Korea
[$]Current address: Department of Neuroscience, Mayo Clinic, Jacksonville, FL, USA
[&]Current address: Division of Pharmacology, Department of Molecular Cell Biology, Sungkyunkwan University School of Medicine, Samsung Biomedical Research Institute, Suwon 446-746, South Korea.

4. Author Contributions:
YX, HSK, TMD and VLD Designed Research, YX, SN, SSK, JNS, BDL, JCG, GC, YL, DS, and LT Performed research and Analyzed Data, YX, SN, TMD and VLD Wrote the Paper.

5. Correspondence should be addressed to (include email address):
Valina L. Dawson (Lead Contact), vdawson@jhmi.edu Neuroregeneration and Stem Cell Programs, Institute for Cell Engineering, Department of Neurology, Johns Hopkins University School of Medicine, 733 N. Broadway, MRB 731, Baltimore, MD 21205, USA

Yulan Xiong, yulanxiong@ksu.edu, Department of Anatomy and Physiology, Kansas

State University College of Veterinary Medicine, 212 Coles Hall, Manhattan, KS 66506, USA

6. Number of Figures: 4

7. Number of Tables: 0

8. Number of Multimedia: 0

9. Number of words for Abstract: 241

10. Number of words for Significance Statement: 118

11. Number of words for Introduction: 402

12. Number of words for Discussion: 555

13. Acknowledgements: Funding Sources

14. Conflict of Interest: Authors report no conflict of interest

15. Funding sources:
This work was supported by grants from NIH/NIA K01-AG046366 (YX), the William N. & Bernice E. Bumpus Foundation Innovation Awards (YX), start-up fund and SUCCESS-FYI Intramural Grant from Kansas State University College of Veterinary Medicine (YX), National Science Foundation Graduate Research Fellowship Award (JCG), Thomas Shortman Training Fund Graduate Scholarship Award (JCG), Axol Science Scholarship Award (JCG), NIH/NINDS NS082205 (HSK), NIH/NINDS NS38377 (HSK, VLD and TMD), and the JPB Foundation (TMD). TMD is the Leonard and Madlyn Abramson Professor in Neurodegenerative Diseases. The authors acknowledge the joint participation by the Adrienne Helis Malvin Medical Research Foundation and the Diana Helis Henry Medical Research Foundation through its direct engagement in the continuous active conduct of medical research in conjunction with The Johns Hopkins Hospital, the Johns Hopkins University School of Medicine and the Foundation's Parkinson's disease Programs.

Key Words: Parkinson’s disease, LRRK2, transgenic mice, α-synuclein

Abstract

Mutations in the leucine-rich repeat kinase 2 (LRRK2) gene have been identified as an unambiguous cause of late-onset, autosomal dominant familial Parkinson’s

disease (PD) and LRRK2 mutations are the strongest genetic risk factor for sporadic PD known to date. A number of transgenic mice expressing wild type or mutant LRRK2 have been described with varying degrees of LRRK2-related abnormalities and modest pathologies. None of these studies directly addressed the role of the kinase domain in the changes observed and none of the mice present with robust features of the human disease. In an attempt to address these issues we created a conditional LRRK2 G2019S (LRRK2 GS) mutant and a functionally negative control, LRRK2 G2019S/D1994A (LRRK2 GS/DA). Expression of LRRK2 GS or LRRK2 GS/DA was conditionally controlled using the tet-off system in which the presence of tetracycline-transactivator protein (tTA) with a CAMKII α promoter (CAMKII α-tTA) induced expression of TetP-LRRK2 GS or TetP-LRRK2 GS/DA in the mouse forebrain. Overexpression of LRRK2 GS in mouse forebrain induced behavioral deficits and α-synuclein pathology in a kinase dependent manner. Similar to other genetically engineered LRRK2 GS mice, there was no significant loss of dopaminergic neurons. These mice provide an important new tool to study neurobiological changes associated with the increased kinase activity from the LRRK2 G2019S mutation which may ultimately lead to a better understanding of not only the physiologic actions of LRRK2, but also potential pathologic actions that underlie LRRK2 GS associated PD.

Significance Statement

Mutations in LRRK2 are the most common genetic cause for both familial and sporadic Parkinson's disease (PD) to date with the G2019S LRRK2 (LRRK2 GS) being the most prevalent mutation. The clinical presentation of patients carrying LRRK2 GS is

111 indistinguishable from sporadic disease in many cases. Many lines of evidence indicate
112 that LRRK2 GS has increased kinase activity and *in vitro* LRRK2 inhibitors or kinase-
113 dead G2019S/D1994A double mutants (LRRK2 GS/DA) reduce LRRK2 GS-mediated
114 toxicity, indicating that LRRK2 associated toxicity is kinase-dependent. However, this
115 concept remains controversial. To address this question *in vivo*, we developed a new
116 tet-inducible conditional transgenic LRRK2 GS and LRRK2 GS/DA mouse model, which
117 exhibits behavioral deficits and α-synuclein pathology in a kinase dependent manner.
118

119 **Introduction**

120 Parkinson's disease (PD) is recognized as the most common movement disorder.
121 The cardinal symptoms are caused by the progressive degeneration of dopaminergic
122 (DA) neurons in the substantia nigra pars compacta (SNpc) (Lees et al., 2009).
123 Mutations in *LRRK2* have been linked to both familial and sporadic forms of PD
124 (Paisan-Ruiz et al., 2004; Zimprich et al., 2004). The LRRK2 protein contains two
125 enzymatic domains, the GTPase and kinase domains, and multiple protein-protein
126 interacting domains including a leucine-rich repeat (LRR), a WD40 repeat, and a
127 LRRK2-specific repeat domain (Cookson, 2010; Mata et al., 2006). The G2019S (GS)
128 mutation within the kinase domain is the most common mutation of LRRK2, which alters
129 LRRK2 GTPase and kinase activities (Lees et al., 2009; Martin et al., 2014b). LRRK2
130 GS mutations lead to alterations in vesicle trafficking, neurite outgrowth, autophagy,
131 cytoskeletal dynamics *in vitro* (Cookson, 2015; Martin et al., 2014b), as well as, defects
132 in protein translation both *in vitro* and *in vivo* (Dorval and Hebert, 2012; Gehrke et al.,
133 2010; Imai et al., 2008; Martin et al., 2014a; Martin et al., 2014b; Martin et al., 2014c).

To study the function of LRRK2 and potential pathologic actions of LRRK2 mutations many lines of transgenic or knock-in mice have been generated. These animal models have provided interesting and valuable biochemical and physiologic insights, but none of these models have recapitulated key features of PD (Beccano-Kelly et al., 2015; Chen et al., 2012; Garcia-Miralles et al., 2015; Herzig et al., 2011; Li et al., 2010; Li et al., 2009; Lin et al., 2009; Liu et al., 2015; Melrose et al., 2010; Ramonet et al., 2011; Tong et al., 2009; Tsika et al., 2014; Volta et al., 2015; Weng et al., 2016; Yue et al., 2015). Interestingly, no animal models have been created to directly test the role of increased kinase activity with the common LRRK2 GS mutation. To address this, we developed a new Tet-inducible conditional LRRK2 mutant G2019S (TetP-LRRK2 GS) transgenic mouse line and a corresponding functionally-negative control G2019S/D1994A (TetP-LRRK2 GS/DA) mouse line under the control of a tetracycline responsive regulator. Crossbreeding the TetP-LRRK2 GS or TetP-LRRK2 GS/DA mice to CamKII α-tTA mice (Mayford et al., 1996) led to high expression levels of LRRK2 GS or the control LRRK2 GS/DA in adult mouse forebrain. High expression of LRRK2 GS induces behavioral deficits and α-synuclein pathology but does not cause significant dopamine neurodegeneration. Nevertheless, these novel transgenic mice offer an excellent platform to explore and elucidate the kinase-dependent actions of LRRK2 in the brain.

Materials and Methods

Animals

Mice were housed and treated in accordance with the National Institutes of Health 'Guide for the Care and Use of Laboratory Animals' and Institutional Animal Care and Use Committees. Animals were housed in a 12 h dark and light cycle with free access to water and food. Both male and female animals were assigned to groups by computer-generated randomization for all experiments. Mice were acclimatized for 3 days in the procedure room before any experiments were started. Sample size was justified by Power analysis.

Generation of conditional *LRRK2* transgenic mouse

A Tandem Affinity Purification (TAP) tag composed of the Streptavidin Binding Peptide (SBP) and Calmodulin Binding Peptide (CBP) was cloned into C-terminal human LRRK2 GS or a LRRK2 GS/DA under the control of a tetracycline responsive regulator (Fig. 1A). The transgenic constructs were linearized by the NotI enzyme and subsequently microinjected into the embryos of B6C3F2 mice. One- or two-cell embryos were transferred into B6D2F1 pseudopregnant female mice. Genomic DNA was prepared from tail snip (Proteinase K, Roche Diagnostics; direct PCR tail Lysis, Viagen) and pups were genotyped by PCR (DreamTaq Green Master Mix, Thermo Scientific) using *TetP-LRRK2* primers (forward: CGG GTC GAG TAG GCG TGT AC; reverse: TCT AGA TGA TCC CCG GGT ACC GAG; PCR product = 173 bp). Positive founders were selected and further subjected to semi quantitative PCR and normalized to GAPDH PCR (forward: AAA CCC ATC ACC ATC TTC CAG; reverse: AGG GGC CAT CCA CAG TCT TCT; PCR product = 300 bp) to screen for high copy-number founders. The three highest copy founders were selected and bred with C57/BL6 mice to generate F1

progeny and to establish the transgenic lines. The following primer sets were used for genotyping of *CamKII α-tTA* (forward: TGA AAG TGG GTC CGC GTA C; reverse: TAC TCG TCA ATT CCA AGG GC; PCR product = 391 bp). LRRK2 induction in conditional transgenic mice was suppressed by feeding the mice with doxycycline-containing food (doxycycline Diet-Sterile, 200 mg per kg doxycycline, Bio-Serv).

Stereological assessment of the number of tyrosine hydroxylase- and Nissl-positive cells.

Mice were perfused with ice-cold phosphate-buffered saline (PBS), followed by 4% paraformaldehyde/PBS (pH 7.4). Brains were removed and post-fixed overnight in the same fixative. After cryoprotection in 30% sucrose/PBS, brains were frozen on dry ice, and serial coronal sections (40 µm sections) were cut with a microtome. Every four sections were collected for subsequent procedures. Free-floating sections were blocked with 4% goat serum (Sigma-Aldrich)/PBS plus 0.3% Triton X-100 and incubated with antibodies to tyrosine hydroxylase (rabbit polyclonal; Novus Biologicals RRID:AB_1218296), followed by incubation with biotin-conjugated antibody to rabbit, ABC reagents (Vector Laboratories) and Sigmafast 3,3-diaminobenzidine (DAB) tablets (Sigma-Aldrich). Sections were counterstained with Nissl (0.09% thionin) after tyrosine hydroxylase staining as previously described (Karuppagounder et al., 2016; Lee et al., 2013). Sections were dehydrated in 100% ethanol and cleared in Xylene (Fisher Scientific) followed by mounting with DPX (Sigma-Aldrich) before imaging under a microscope. TH-positive and Nissl positive DA neurons from the SNpc region were counted through an optical fractionator, the unbiased method for cell counting. This

unbiased stereological counting was carried out by a computer-assisted image analysis system consisting of an Axiophot photomicroscope (Carl Zeiss Vision) equipped with a computer-controlled motorized stage (Ludl Electronics), a Hitachi HV C20 video camera and Stereo Investigator software (MicroBrightField). Fiber density in the striatum was quantified by optical density (OD). Image J software (NIH) was used to analyze the OD as previously described (Karuppagounder et al., 2016).

Western blotting

Brain extracts from indicated genotype were prepared by homogenization in lysis buffer [1 X phosphate-buffered saline, 1% Triton X-100, 1 X Complete protease inhibitor (4693116001, Sigma), 1 X PhosSTOP phosphatase inhibitor (4906845001; Sigma)]. Protein concentration was determined by BCA method (Pierce Biotech). About 100 µg of protein was resolved by sodium dodecyl sulfate–polyacrylamide gel electrophoresis, transferred to polyvinylidene fluoride (PVDF) membrane and probed with mouse anti-LRRK2 antibody (N136/8, NeuroMab RRID:AB_2234791) or rabbit anti-LRRK2 antibody (1304; D18E12, Cell Signaling Technology) recognizing both mouse and human LRRK2. Membrains were also probed with rabbit anti-LRRK2 phospho Ser1292 antibody (ab203181; MJFR-19-7-8, Abcam), or with mouse anti-α-synuclein antibody (610787; BD Transduction Laboratories; RRID:AB_398108) or rabbit anti-α-synuclein antibody (2642; Cell Signaling Technology; RRID:AB_2192679), or with anti-actin-peroxidase rabbit polyclonal antibody for loading control (A3854; Sigma-Aldrich; RRID:AB_262011). Densitometric analysis was conducted to quantify the fold overexpression of LRRK2 relative to endogenous mouse LRRK2. Total LRRK2 protein

levels were normalized to actin and expressed as the percent of non-transgenic (Tg) controls. Mean values from three mice per genotype/control were analyzed for statistical significance by two-tailed unpaired Student's *t*-test compared with non-Tg controls.

Open field test and d-amphetamine administration

Spontaneous locomotor and exploratory activities were assessed in open field square-shaped (16 X 16) chambers equipped with an automated photobeam tracking system (San Diego Instruments, San Diego, CA, USA). Briefly, a mouse was placed in the center of the open field arena and allowed to explore the area for 25 min, following by d-amphetamine injection (7 mg/kg s.c.) (A-5880 Lot #: 34H0145 Sigma-Aldrich) and another 25 min exploration. The activities of a mouse were recorded every minute by Photobeam Activity System (PAS) software installed on a computer connected to the open field equipment. Before and after each testing, the clear acrylic enclosure of the surface of the arena was cleaned with 70% ethanol. The total number of beam breaks during the total 50 min period was used to determine gross locomotor activity of a mouse.

Rotarod test

Motor coordination of mice was measured as the retention time on an accelerating rotarod of the rotamex V instrument equipped with photobeams and a sensor to automatically detect mice that fell from the rotarod (Columbus Instruments, Columbus, OH). Before the actual test the mice were trained on the rotarod at 4.0 to 40 r.p.m. for 5 min and allowed to rest for at least 30 min. The training occurred over three consecutive

days and consists of three test trials. On the day of the test, four mice were placed on separate rods and the durations on the accelerating rods were recorded automatically by the software installed on a computer connected to the instrument. The setting of the rotamex was: Start speed, 4.0 r.p.m.; maximum speed, 40 r.p.m.; acceleration interval, 30 s; acceleration step, 4 r.p.m., and the setting remained constant throughout all trials. The tests were blinded and evaluated in three sessions and the average retention time and end speed were recorded for each mouse. The retention time was used to determine the motor coordination of the mouse.

Pole test

The pole consists of a 2.5 ft metal rod with a 9 mm diameter that is wrapped with bandage gauze. Briefly, the mice were placed 3 inches from the top of the pole facing head-up. Total time taken to turn and reach the base of the pole was recorded. Before the actual test the mice were trained for three consecutive days and each training session consisted of three test trials. On the day of the test, mice were evaluated in three sessions with one hour intervals in between, and total times were recorded. Results were expressed in total time in seconds (Karuppagounder et al., 2016)

Statistical analysis

Two-way ANOVA and two-tailed unpaired Student's *t* test was used for data analysis. Data represent mean ± SEM, and $p \leq 0.05$ was considered statistically significant. *p <0.05, **p < 0.01, ***p < 0.001. Power analysis was performed by using G*Power 3.1

software to determine approximate sample sizes for behavior tests or stereological analysis.

Results

Generation of TET-inducible conditional LRRK2 transgenic mice. We generated tetracycline responsive transgenic mice (TetP-LRRK2 GS or TetP-LRRK2 GS/DA) using C-terminal tandem affinity purification (TAP) tagged human LRRK2 GS or LRRK2 GS/DA under the control of a tetracycline responsive regulator (Fig. 1A). 27 TetP-LRRK2 GS founders and 33 TetP-LRRK2 GS/DA founder mice were identified by PCR screening for the tetracycline promoter (Fig. 1B, C). Three male mice with the highest copy number were selected as founders and crossbred to CamKII α-tTA transgenic mice (Mayford et al., 1996) (Fig. 1D). Dams were maintained on doxycycline food until pups were weaned to prevent expression of transgenes and possible compensation during development. Mice expressing both CamKII α-tTA and TetP-LRRK2 GS or TetP-LRRK2 GS/DA were identified by PCR (Fig. 1E). At approximately 2 months of age, doxycycline food was withdrawn and overexpression of LRRK2 GS or LRRK2 GS/DA was monitored. LRRK2 GS is overexpressed 16, 5, 2-fold in line 569, 648 and 597, respectively and LRRK2 GS/DA is overexpressed 6, 15, 3-fold in line 767, 763 and 768 respectively (Fig. 1F, G). Since line 569 and line 763 overexpress LRRK2 at similar levels they were selected for further study. A regional assessment of the overexpression of LRRK2 GS (line 569) and LRRK2 GS/DA (line 763) were monitored by western blot analysis (Fig. 1H, I). LRRK2 GS or GS/DA is overexpressed about 5, 15, 17, 9, 4-Fold in the olfactory bulb (OB), cortex (CTX), striatum (STR), hippocampus (HIP) and ventral

midbrain (VMB), respectively, while there is no significant change in LRRK2 expression in the brain stem (BS) and cerebellum (CER) (Fig. 1H, I). Collectively, LRRK2 was induced at very high levels in the mouse forebrain. To monitor LRRK2 kinase activity and confirm that LRRK2 GS/DA is kinase dead *in vivo*, the phosphorylation status of LRRK2 was examined in LRRK2 GS and LRRK2 GS/DA mice by LRRK2 phosphor S1292 antibody (Fig. 1J, K). Western blots of total protein from mouse brains of control, LRRK2 GS and LRRK2 GS/DA revealed that LRRK2 GS has high phosphorylation level and LRRK2 GS/DA does not have a detectable kinase activity (Fig. 1J, K).

Behavioral deficits of conditional LRRK2-G2019S transgenic mice. The potential effects of LRRK2 GS expression on motor behavior was assessed. Open field, pole test and rotarod testing were performed with LRRK2 GS and LRRK2 GS/DA transgenic mice. LRRK2 GS and LRRK2 GS/DA transgenic mice performed similarly as non-transgenic control mice under normal conditions in the open field test at 10, 15 and 22 months of age (Fig. 2A and data not shown). There was no significant difference between LRRK2 GS and LRRK2 GS/DA at 10 and 15 months of age (data not shown). Interestingly, LRRK2 GS mice have a blunted response to d-amphetamine administration (7 mg/kg s.c.) at 22 months whereas non-transgenic and LRRK2 GS/DA mice exhibit increased activity (Fig. 2A). In the dopamine-sensitive pole test assessed at 22 months of age, LRRK2 GS transgenic mice had an insignificant deficit in ability to descend the pole ($p=0.0514$). The LRRK2 GS/DA performed similar to non-transgenic control mice (Fig. 2B). In the rotarod test, both the LRRK2 GS and LRRK2 GS/DA transgenic mice performed normally at 10, 15 and 22 months of age (Fig. 2C and data

316 not shown). Taken together, these results indicate that the LRRK2 GS mice have no
317 robust DA sensitive behavioral deficits.
318
319 **Conditional LRRK2-G2019S transgenic mice exhibit normal nigrostriatal**
320 **dopaminergic pathway**. To determine whether temporal overexpression of LRRK2 GS
321 in the mouse forebrain induces degeneration of midbrain DA neurons, we assessed DA
322 neuronal number by unbiased stereological counting of TH and Nissl positive neurons at
323 22 months of age. No significant DA neuronal loss was observed (Fig. 3A,B,C).
324 Dopaminergic neurons are of normal size and morphology in the substantia nigra of
325 LRRK2 GS mice (Fig. 3A). The fiber density of TH-positive dopaminergic nerve
326 terminals in the striatum are unaltered in LRRK2 GS mice at 22 months of age (Fig. 3D,
327 E). Taken together our data suggest that the high levels of expression of LRRK2 GS in
328 mouse forebrain are not sufficient to induce degeneration of dopaminergic neurons of
329 the nigrostriatal dopaminergic pathway with advancing age. These findings are
330 consistent with the behavioral data.
331
332 **α-Synuclein pathology in conditional LRRK2-G2019S transgenic mice**. Since the
333 majority of patients carrying the LRRK2 GS mutation have α-synuclein positive Lewy
334 bodies and increased levels of phospho-serine 129 (pS129) α-synuclein, the status of
335 endogenous α-synuclein was monitored in the non-transgenic control, LRRK2 GS and
336 LRRK2 GS/DA mice. Immunoblot analysis for α-synuclein in the Triton-X100 soluble
337 fraction reveals no substantial difference in the immunoreactivity for α-synuclein (Fig.
338 4A) and no detectable immunoreactivity for pS129 α-synuclein (data not shown) at 22

months between LRRK2 GS mice and LRRK2 GS/DA mice. In the Triton-X100 insoluble fraction, the observed high molecular weight species (above 75 kD) of α-synuclein are indicative of aggregation and are similar between LRRK2 GS and LRRK2 GS/DA mice in the ventral midbrain (VMB), brain stem (BS) and cerebellum (CER) regions but are significantly increased in the olfactory bulb (OB), cortex (CTX), striatum (STR) and hippocampus (HIP) of LRRK2 GS mice at 22 months of age compared to LRRK2 GS/DA and non-Tg control mice (Fig. 4B, C). Moreover, in the Triton-X100 insoluble fraction, low and similar levels of immunoreactivity for pS129 α-synuclein are observed in STR, VMB, BS and CER brain regions of non-Tg mice, LRRK2 GS and LRRK2 GS/DA mice. In contrast, pS129 α-synuclein levels are significantly increased in OB, CTX and HIP brain regions of 22-month-old LRRK2 GS mice compared to LRRK2 GS/DA and non-Tg control mice of the same age (Fig. 4B, D). No significant difference in the immunoreactivity for α-synuclein and pS129 α-synuclein in both Triton-X100 soluble and insoluble fractions was observed at the age of 10 and 15 months among LRRK2 GS, GS/DA and non-Tg control mice (data not shown). This observation suggests that the LRRK2 GS mutation can promote α-synuclein pathology in a kinase and age dependent manner.

Discussion

It is well established that the disease causing LRRK2 GS mutation exhibits increased kinase activity for both autophosphorylation and hyperphosphorylation of LRRK2 kinase substrates. While LRRK2 kinase inhibitors or kinase-dead G2019S/D1994A double mutants reduce LRRK2 GS-mediated toxicity indicating that

LRRK2 toxicity is kinase-dependent (Cookson, 2015; Martin et al., 2014b). This conclusion remains controversial and alternative hypotheses have been suggested (Skibinski et al., 2014). To define the kinase dependent and kinase independent pathophysiologic actions of LRRK2 additional models are needed. Thus, we generated a conditional tet-off LRRK2 G2019S (LRRK2 GS) mutant and a functionally negative control, LRRK2 G2019S/D1994A (LRRK2 GS/DA) driven by the CAMKIIα promoter. Overexpression of LRRK2 GS in mouse forebrain induced behavioral deficits and α-synuclein pathology in a kinase dependent manner whereas these events were absent in the LRRK2 GS/DA mice. However, consistent with other genetically engineered LRRK2 GS mice there was no significant loss of dopaminergic neurons.

Since the majority of LRRK2 PD patients exhibit α-synuclein aggregation, the role of LRRK2 in α-synuclein pathology in different LRRK2 mouse models has been explored. Lin *et al.* showed that overexpression of LRRK2 in mouse forebrain promotes the abnormal aggregation of exogenously overexpressed α-synuclein and knockout of LRRK2 rescued A53T α-synuclein overexpression induced abnormalities (Lin et al., 2009). However, Tong *et al.* demonstrated that LRRK2 knockout mice present with a robust aggregation of α-synuclein while Daher *et al.* showed that knockout of LRRK2 has no influence on A53T α-synuclein induced neurodegeneration (Daher et al., 2012; Tong et al., 2010). The different findings between these studies could be due to the different α-synuclein expression levels or technical concerns. Our LRRK2 mouse model for provides the first evidence that overexpression of LRRK2 in mouse forebrain induces endogenous α-synuclein aggregation and increased pS129 α-synuclein levels, which occur in a kinase dependent manner. Whether LRRK2 could be employed as a

385 therapeutic target for α-synuclein-mediated neurodegeneration remains to be
386 elucidated.

387 The reasons why past rodent models of the LRRK2 GS mutation as well as our
388 new transgenic mouse model do not exhibit nigral neurodegeneration is not known
389 although many alpha-synuclein based mouse models also lack nigral neurodegeneation
390 (Lee, et al., 2012). Possibilities include compensatory mechanisms, levels of expression
391 that are higher in brain regions other than the ventral midbrain or substantia nigra, poor
392 expression in the substantia nigra, or lack of expression of the LRRK2 GS mutation in
393 cell types other than neurons such as astrocytes or microglia.

394 All of these possibilities should be taken into consideration in developing new
395 LRRK2 animal models meant to study neurodegeneration. The lack of
396 neurodegeneration does not diminish the value of these models for biochemical
397 investigations of the function of LRRK2. When coupled with the ability to purify the
398 LRRK2 protein complex via the TAP tag, our new mouse model permit the investigation
399 of increased kinase activity on LRRK2 biologic substrates and outcomes. Overall, these
400 mice provide an important new tool to study neurobiologic changes that are due to the
401 over activation of the kinase activity by the LRRK2 GS mutation, which may lead to a
402 better understanding of not only the physiological functions of LRRK2, but also the
403 potential pathologic mechanisms underlying LRRK2 GS-associated PD.

404

405 **References**

406 Beccano-Kelly, D.A., Volta, M., Munsie, L.N., Paschall, S.A., Tatarnikov, I., Co, K.,
407 Chou, P., Cao, L.P., Bergeron, S., Mitchell, E., *et al.* (2015). LRRK2

overexpression alters glutamatergic presynaptic plasticity, striatal dopamine tone, postsynaptic signal transduction, motor activity and memory. Hum Mol Genet *24*, 1336-1349.

Chen, C.Y., Weng, Y.H., Chien, K.Y., Lin, K.J., Yeh, T.H., Cheng, Y.P., Lu, C.S., and Wang, H.L. (2012). (G2019S) LRRK2 activates MKK4-JNK pathway and causes degeneration of SN dopaminergic neurons in a transgenic mouse model of PD. Cell Death Differ *19*, 1623-1633.

Cookson, M.R. (2010). The role of leucine-rich repeat kinase 2 (LRRK2) in Parkinson's disease. Nat Rev Neurosci *11*, 791-797.

Cookson, M.R. (2015). LRRK2 Pathways Leading to Neurodegeneration. Curr Neurol Neurosci Rep *15*, 42.

Daher, J.P., Pletnikova, O., Biskup, S., Musso, A., Gellhaar, S., Galter, D., Troncoso, J.C., Lee, M.K., Dawson, T.M., Dawson, V.L.*, et al.* (2012). Neurodegenerative phenotypes in an A53T alpha-synuclein transgenic mouse model are independent of LRRK2. Hum Mol Genet *21*, 2420-2431.

Dorval, V., and Hebert, S.S. (2012). LRRK2 in Transcription and Translation Regulation: Relevance for Parkinson's Disease. Front Neurol *3*, 12.

Garcia-Miralles, M., Coomaraswamy, J., Habig, K., Herzig, M.C., Funk, N., Gillardon, F., Maisel, M., Jucker, M., Gasser, T., Galter, D.*, et al.* (2015). No dopamine cell loss or changes in cytoskeleton function in transgenic mice expressing physiological levels of wild type or G2019S mutant LRRK2 and in human fibroblasts. PLoS One *10*, e0118947.

Gehrke, S., Imai, Y., Sokol, N., and Lu, B. (2010). Pathogenic LRRK2 negatively regulates microRNA-mediated translational repression. Nature *466*, 637-641.

Herzig, M.C., Kolly, C., Persohn, E., Theil, D., Schweizer, T., Hafner, T., Stemmelen, C., Troxler, T.J., Schmid, P., Danner, S.*, et al.* (2011). LRRK2 protein levels are determined by kinase function and are crucial for kidney and lung homeostasis in mice. Hum Mol Genet *20*, 4209-4223.

Imai, Y., Gehrke, S., Wang, H.Q., Takahashi, R., Hasegawa, K., Oota, E., and Lu, B. (2008). Phosphorylation of 4E-BP by LRRK2 affects the maintenance of dopaminergic neurons in Drosophila. EMBO J *27*, 2432-2443.

Karuppagounder, S.S., Xiong, Y., Lee, Y., Lawless, M.C., Kim, D., Nordquist, E., Martin, I., Ge, P., Brahmachari, S., Jhaldiyal, A.*, et al.* (2016). LRRK2 G2019S transgenic mice display increased susceptibility to 1-methyl-4-phenyl-1,2,3,6-tetrahydropyridine (MPTP)-mediated neurotoxicity. J Chem Neuroanat *76*, 90-97.

Lee, Y., Dawson V.L., and Dawson, T.M. (2012). Animal Models of Parkinson's disease: Vertebrate genetics. Cold Spring Harb Perspect Med *2,* a009324 10.1101/cshperspect.a009324

Lee, Y., Karuppagounder, S.S., Shin, J.H., Lee, Y.I., Ko, H.S., Swing, D., Jiang, H., Kang, S.U., Lee, B.D., Kang, H.C.*, et al.* (2013). Parthanatos mediates AIMP2-activated age-dependent dopaminergic neuronal loss. Nat Neurosci *16*, 1392-1400.

Lees, A.J., Hardy, J., and Revesz, T. (2009). Parkinson's disease. Lancet *373*, 2055-2066.

452 Li, X., Patel, J.C., Wang, J., Avshalumov, M.V., Nicholson, C., Buxbaum, J.D., Elder,
453 G.A., Rice, M.E., and Yue, Z. (2010). Enhanced striatal dopamine transmission
454 and motor performance with LRRK2 overexpression in mice is eliminated by
455 familial Parkinson's disease mutation G2019S. J Neurosci *30*, 1788-1797.
456 Li, Y., Liu, W., Oo, T.F., Wang, L., Tang, Y., Jackson-Lewis, V., Zhou, C., Geghman, K.,
457 Bogdanov, M., Przedborski, S.*, et al.* (2009). Mutant LRRK2(R1441G) BAC
458 transgenic mice recapitulate cardinal features of Parkinson's disease. Nat Neurosci
459 *12*, 826-828.
460 Lin, X., Parisiadou, L., Gu, X.L., Wang, L., Shim, H., Sun, L., Xie, C., Long, C.X., Yang,
461 W.J., Ding, J.*, et al.* (2009). Leucine-rich repeat kinase 2 regulates the progression
462 of neuropathology induced by Parkinson's-disease-related mutant alpha-synuclein.
463 Neuron *64*, 807-827.
464 Liu, G., Sgobio, C., Gu, X., Sun, L., Lin, X., Yu, J., Parisiadou, L., Xie, C., Sastry, N.,
465 Ding, J.*, et al.* (2015). Selective expression of Parkinson's disease-related
466 Leucine-rich repeat kinase 2 G2019S missense mutation in midbrain dopaminergic
467 neurons impairs dopamine release and dopaminergic gene expression. Hum Mol
468 Genet *24*, 5299-5312.
469 Martin, I., Abalde-Atristain, L., Kim, J.W., Dawson, T.M., and Dawson, V.L. (2014a).
470 Abberant protein synthesis in G2019S LRRK2 Drosophila Parkinson disease-
471 related phenotypes. Fly (Austin) *8*, 165-169.
472 Martin, I., Kim, J.W., Dawson, V.L., and Dawson, T.M. (2014b). LRRK2 pathobiology in
473 Parkinson's disease. J Neurochem *131*, 554-565.

474 Martin, I., Kim, J.W., Lee, B.D., Kang, H.C., Xu, J.C., Jia, H., Stankowski, J., Kim, M.S.,
475 Zhong, J., Kumar, M.*, et al.* (2014c). Ribosomal protein s15 phosphorylation
476 mediates LRRK2 neurodegeneration in Parkinson's disease. Cell *157*, 472-485.
477 Mata, I.F., Wedemeyer, W.J., Farrer, M.J., Taylor, J.P., and Gallo, K.A. (2006). LRRK2
478 in Parkinson's disease: protein domains and functional insights. Trends Neurosci
479 *29*, 286-293.
480 Mayford, M., Bach, M.E., Huang, Y.Y., Wang, L., Hawkins, R.D., and Kandel, E.R.
481 (1996). Control of memory formation through regulated expression of a CaMKII
482 transgene. Science *274*, 1678-1683.
483 Melrose, H.L., Dachsel, J.C., Behrouz, B., Lincoln, S.J., Yue, M., Hinkle, K.M., Kent,
484 C.B., Korvatska, E., Taylor, J.P., Witten, L.*, et al.* (2010). Impaired dopaminergic
485 neurotransmission and microtubule-associated protein tau alterations in human
486 LRRK2 transgenic mice. Neurobiol Dis *40*, 503-517.
487 Paisan-Ruiz, C., Jain, S., Evans, E.W., Gilks, W.P., Simon, J., van der Brug, M., Lopez
488 de Munain, A., Aparicio, S., Gil, A.M., Khan, N.*, et al.* (2004). Cloning of the gene
489 containing mutations that cause PARK8-linked Parkinson's disease. Neuron *44*,
490 595-600.
491 Ramonet, D., Daher, J.P., Lin, B.M., Stafa, K., Kim, J., Banerjee, R., Westerlund, M.,
492 Pletnikova, O., Glauser, L., Yang, L.*, et al.* (2011). Dopaminergic neuronal loss,
493 reduced neurite complexity and autophagic abnormalities in transgenic mice
494 expressing G2019S mutant LRRK2. PLoS One *6*, e18568.

495 Skibinski, G., Nakamura, K., Cookson, M.R., and Finkbeiner, S. (2014). Mutant LRRK2
496 toxicity in neurons depends on LRRK2 levels and synuclein but not kinase activity
497 or inclusion bodies. J Neurosci *34*, 418-433.
498 Tong, Y., Pisani, A., Martella, G., Karouani, M., Yamaguchi, H., Pothos, E.N., and Shen,
499 J. (2009). R1441C mutation in LRRK2 impairs dopaminergic neurotransmission in
500 mice. Proc Natl Acad Sci U S A *106*, 14622-14627.
501 Tong, Y., Yamaguchi, H., Giaime, E., Boyle, S., Kopan, R., Kelleher, R.J., 3rd, and
502 Shen, J. (2010). Loss of leucine-rich repeat kinase 2 causes impairment of protein
503 degradation pathways, accumulation of alpha-synuclein, and apoptotic cell death in
504 aged mice. Proc Natl Acad Sci U S A *107*, 9879-9884.
505 Tsika, E., Kannan, M., Foo, C.S., Dikeman, D., Glauser, L., Gellhaar, S., Galter, D.,
506 Knott, G.W., Dawson, T.M., Dawson, V.L.*, et al.* (2014). Conditional expression of
507 Parkinson's disease-related R1441C LRRK2 in midbrain dopaminergic neurons of
508 mice causes nuclear abnormalities without neurodegeneration. Neurobiol Dis *71*,
509 345-358.
510 Volta, M., Cataldi, S., Beccano-Kelly, D., Munsie, L., Tatarnikov, I., Chou, P., Bergeron,
511 S., Mitchell, E., Lim, R., Khinda, J.*, et al.* (2015). Chronic and acute LRRK2
512 silencing has no long-term behavioral effects, whereas wild-type and mutant
513 LRRK2 overexpression induce motor and cognitive deficits and altered regulation
514 of dopamine release. Parkinsonism Relat Disord *21*, 1156-1163.
515 Weng, Y.H., Chen, C.Y., Lin, K.J., Chen, Y.L., Yeh, T.H., Hsiao, I.T., Chen, I.J., Lu,
516 C.S., and Wang, H.L. (2016). (R1441C) LRRK2 induces the degeneration of SN

dopaminergic neurons and alters the expression of genes regulating neuronal survival in a transgenic mouse model. Exp Neurol *275 Pt 1*, 104-115.

Yue, M., Hinkle, K.M., Davies, P., Trushina, E., Fiesel, F.C., Christenson, T.A., Schroeder, A.S., Zhang, L., Bowles, E., Behrouz, B.*, et al.* (2015). Progressive dopaminergic alterations and mitochondrial abnormalities in LRRK2 G2019S knock-in mice. Neurobiol Dis *78*, 172-195.

Zimprich, A., Biskup, S., Leitner, P., Lichtner, P., Farrer, M., Lincoln, S., Kachergus, J., Hulihan, M., Uitti, R.J., Calne, D.B.*, et al.* (2004). Mutations in LRRK2 cause autosomal-dominant parkinsonism with pleomorphic pathology. Neuron *44*, 601-607.

Figure 1. Generation of TET-inducible conditional LRRK2 transgenic mice. ***A,*** Schematic diagram of the TetP-LRRK2-TAP construct. ***B***. Relative transgene copy number determined by semi-quantitative PCR performed on genomic DNA expressed in arbitrary units as the ratio of the TetP-LRRK2-G2019S (GS) transgene to GAPDH for each founder mouse. ***C,*** Relative transgene copy number determined by semi-quantitative PCR performed on genomic DNA expressed in arbitrary units as the ratio of the TetP-LRRK2-GS2019S/D1994A (GS/DA) transgene to GAPDH for each founder mouse. ***D***, Schematic diagram of the generation of LRRK2 inducible transgenic mice using the "tet-off" system. ***E,*** Representative genotyping PCR for TetP-LRRK2 and CamKIIα-tTA using genomic DNA. GAPDH PCR was used as an internal control. ***F,*** Western blot analysis of LRRK2 expression from LRRK2 transgenic mouse brain. Each number represents a single LRRK2 transgenic founder line: 569, 648 and 597 of LRRK2-GS, 767, 763 and 768 LRRK2-GS/DA transgenic mice. ***G,*** Quantification of LRRK2 expression in mouse brains normalized to β-actin, n=3. Differences between transgenic and control groups were assessed by unpaired, two-tailed Student's *t*-test**.** Quantified data are expressed as mean ± SEM. **P* < 0.05, ****P* < 0.001. ***H,*** Representative western blots of LRRK2 distribution in brain subregions from control and LRRK2-GS (line 569) and LRRK2-GS/DA (line 763) transgenic mice (OB, olfactory bulb; CTX, cortex; STR, striatum; HIP, hippocampus; VMB, ventral midbrain; BS, brain stem; CER, cerebellum). ***I,*** Quantification of LRRK2 distribution in mouse brains normalized to β-actin, n = 3. ***J***, Western blot analysis of total protein from mouse brains of control, LRRK2 GS and LRRK2 GS/DA by anti-LRRK2 and LRRK2 phosphor S1292 antibodies.

K, Quantification of phosphor Ser1292 LRRK2 levels in mouse brains normalized to total LRRK2 protein level, n=3. Quantified data are expressed as mean ± SEM, **P* < 0.05, ***P* < 0.01, ****P* < 0.001, Differences between transgenic and control groups for were assessed by two-way ANOVA**.** Non-significant difference between LRRK2 GS and LRRK2 GS/DA groups.

Figure 2. Behavioral deficits of conditional LRRK2-G2019S transgenic mice. *A,* Open field analysis under normal conditions and following amphetamine challenge. Mice were placed in the center of the open field arena and allowed to explore the area for 25 min, following by d-amphetamine injection (7 mg/kg s.c.) and another 25 min exploration. The total activities of mice were recorded every minute (Control n=7, GS n=9, GS/DA n=8). ***B,*** Pole test to monitor the behavioral abnormalities of 22 month old LRRK2 GS and GSDA transgenic and age-matched littermate controls (Control n=8, GS n=8, GS/DA n=7). ***C,*** Assessment of latency to fall in an accelerated rotarod test (Control n=8, GS n=9, GS/DA n=8). Data are the means ± SEM. Statistical significance was determined by two-way ANOVA. **p* <0.05 n.s.: non-significant.

Figure 3. Characterization of the nigrostriatal pathway of LRRK2 conditional transgenic mice. ***A,*** Representative tyrosine hydroxylase (TH) immunohistochemistry of the midbrain coronal sections of 22 month-old LRRK2 GS and GSDA transgenic and age-matched littermate controls. ***B, C,*** Stereological assessment of (B) TH and(C) Nissl positive neurons in the SNpc (Control n=9, GS n=9, GS/DA n=9). Data are the mean number of cells per region ± SEM, n = 9 mice per group. Statistical significance was determined by two-tailed unpaired Student's *t* test. ***D,*** Representative images of TH

574 immunostaining of nerve terminals in the striatum of LRRK2 conditional transgenic mice
575 at 22 months. ***E,*** Quantitation of TH immunostaining in the striatum using Image J
576 software (NIH) (Control n=7, GS n=7, GS/DA n=7). Differences between groups were
577 assessed by two-way ANOVA, Bars represent the mean ± SEM ($n \geq 5$
578 animals/genotype). n.s.: non-significant.
579
580 **Figure 4. The levels of α-synuclein aggregation in the LRRK2 GS and LRRK2**
581 **GSDA mice**. ***A,*** Representative immunoblots of α-syn and β-actin in the Triton-X100
582 (TX)-soluble fraction of different brain regions from 22-month-old transgenic mice and
583 age-matched littermate non-Tg controls. ***B,*** Representative immunoblots of α-syn and
584 β-actin in the TX-insoluble fraction of different brain regions from 22-month-old
585 transgenic mice and age-matched littermate non-Tg controls. In the insoluble fractions,
586 high molecular weight (75 kD) species of α-synuclein are detected in OB, CTX, STR,
587 HIP, but not VMB, BS and CER of LRRK2 GS mice. ***C,*** Quantification of high molecular
588 weight (HMW) α-syn protein levels in ***B*** normalized to β-actin. (Control n=3, GS n=3,
589 GS/DA n=3). ***D***. Quantification of pS129 α-syn protein levels in ***B*** normalized to α-syn
590 monomer (17KD). (Control n=3, GS n=3, GS/DA n=3). Differences between LRRK2 GS
591 versus Control or LRRK2 GS/DA groups were assessed by two-way ANOVA, Bars
592 represent the mean ± SEM. *$P < 0.05$, **$P < 0.01$, ***$P < 0.001$. Non-significant
593 difference between LRRK2 GS/DA and control groups.
594
595
596

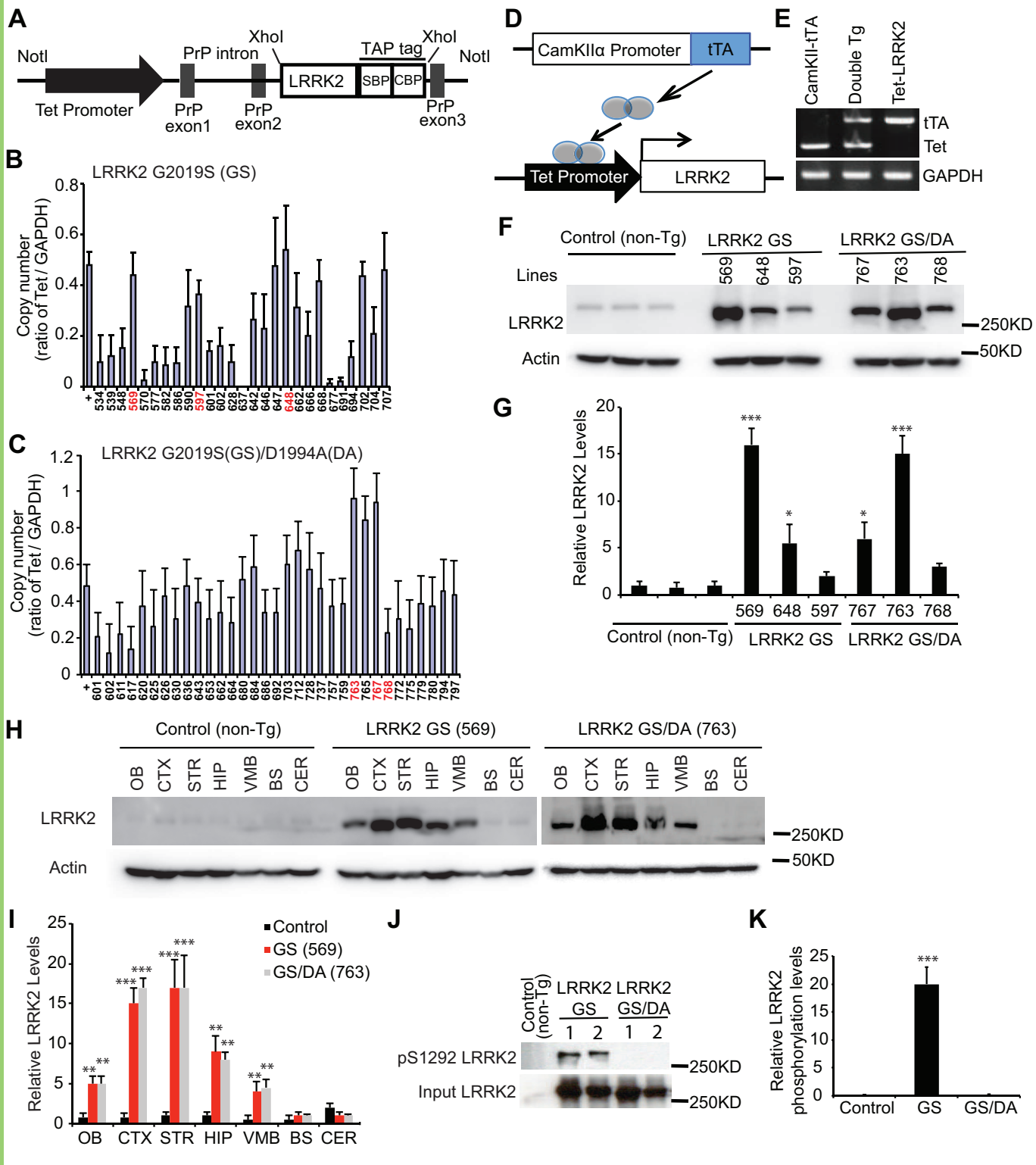

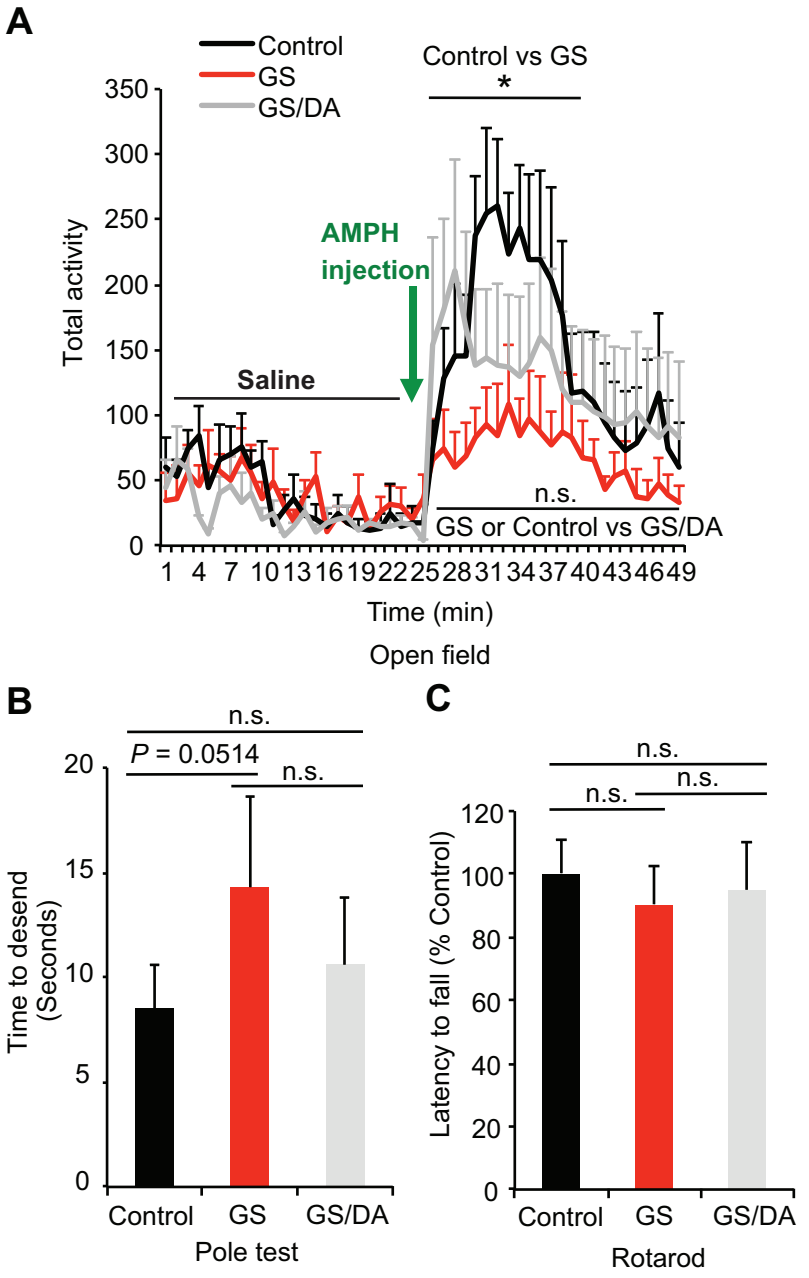

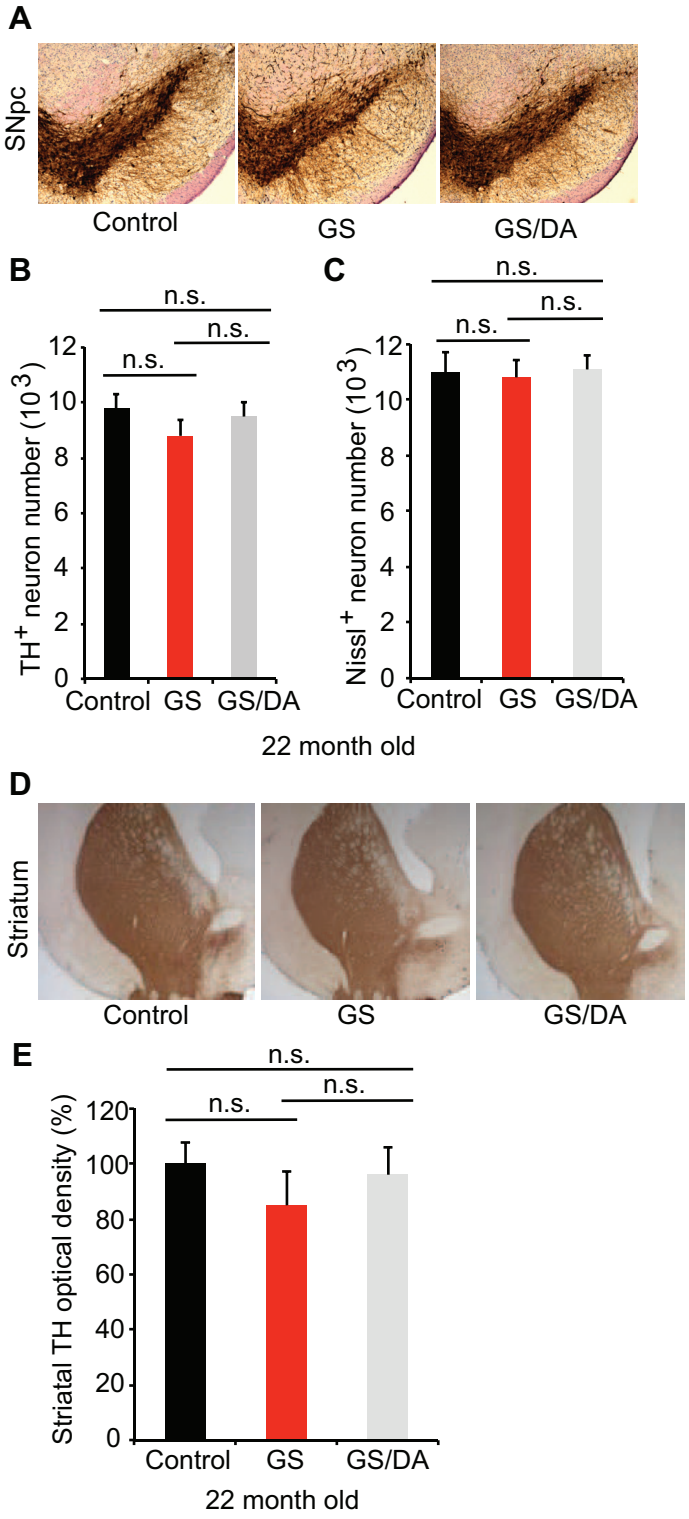

Fig.4